Alumina Recovery from Sodium Aluminate Solutions via Carbonation

Danai Marinos[1], Dimitrios Kotsanis[2], Casper Van der Eijk[3] and Efthymios Balomenos[4] and Dimitrios Panias[5]
1. PhD student
2. Materials Characterization Specialist
4. Assistant Professor
5. Professor
NTUA - Technologies for Sustainable Metallurgy - Laboratory of Metallurgy, Athens, Greece
3. Senior Research Scientist
SINTEF Industry - Department of Metal Production and Processing, Trondheim, Norway
Corresponding author: dmarinou@metal.ntua.gr
https://doi.org/10.71659/icsoba2025-aa009

Abstract

This study explores the recovery of alumina from sodium aluminate, sodium carbonate, and sodium hydroxide solutions resulting from the leaching of calcium aluminate slags generated from pyrometallurgical reduction of various ores/by-products for metallic iron, silicon, and manganese extraction within several EU-funded projects. Such calcium aluminate slags are leached with sodium carbonate, generating a pregnant leaching solution. The entire process is evaluated starting from the carbonation of the pregnant leaching solution, where alumina hydrates (aluminium hydroxides) are precipitated by purging carbon dioxide gas into the solution. The alumina hydrates are calcined to produce alumina (aluminium oxide), which is used for its dissolution in cryolite.

The research aims to highlight the key characteristics of this process and the challenges involved in producing smelter-grade alumina. In addition, critical aspects of the process, such as the removal of sodium ions from the hydrated precipitate, are assessed. These are instrumental in attaining the purity and quality of the alumina hydrate. The findings demonstrate the viability of processing industrial by-products into useful products with reduced environmental impact. This study provides information on the efficiency of carbonation and facilitates the development of more sustainable alumina production from alternative raw materials.

Keywords: Alumina hydrates, Alumina, Carbonation precipitation, Calcination, Cryolite dissolution.

1. Introduction

Aluminothermic processes are emerging as promising alternatives to traditional carbothermic reduction methods [1]. Unlike carbothermic reduction, which relies on carbon-based reductants and results in significant CO_2 emissions, aluminothermic reduction employs aluminium, preferably sourced from scrap or dross, as a reductant. This approach can substantially lower the greenhouse gas emissions, particularly if the aluminium used can be recovered downstream.

Depending on the process, calcium aluminate (CA) slags are a by-product of aluminothermic reduction processes. They are generated when aluminium reacts with oxides like dicalcium silicate slag, iron oxide, or other metal oxides in the presence of a calcium source. CA slags can also be produced from bauxite residue smelting for iron recovery. The composition and structure of CA slags can vary, but they typically contain significant quantities of aluminium oxide and depending on their phase composition and cooling conditions, can serve as secondary alumina

sources. Efficient utilization of CA slags is crucial to maximizing resource recovery, minimizing waste, and promoting a circular economy [2].

CA slags can be leached with a sodium carbonate (Na_2CO_3) solution to produce a pregnant leaching solution (PLS), rich in sodium aluminate and a solid residue predominantly composed of calcium carbonate. Although this solution is often supersaturated, its alumina concentration (15–70 g/L Al_2O_3) is lower than that typically found in Bayer liquors (85–165 g/L Al_2O_3) [3]. In the Bayer process, only a relatively small portion of alumina is recovered via cooling crystallization; the rest remains in the recycled liquor. In contrast, carbonation, through pH-driven precipitation, can achieve high alumina recoveries, enhancing process productivity. Furthermore, CO_2 addition regenerates the Na_2CO_3 solution, allowing it to be reused for fresh slag leaching. Leaching CA slags with Na_2CO_3 yields a complex alkaline PLS, primarily composed of sodium aluminate ($NaAl(OH)_4$), sodium carbonate, and sodium hydroxide. The simplified leaching reaction – similar to the liquor causticization – done in the Bayer process is shown in Equation 1, though it varies with the specific CA phases:

$$CaO \cdot Al_2O_{3(s)} + Na_2CO_{3(aq)} + H_2O_{(l)} \rightarrow 2NaOH_{(aq)} + NaAlO_{2(aq)} + CaCO_3 \downarrow \quad (1)$$

When the resulting PLS is carbonated, alumina hydrates precipitate according to Equations 2–5. These reactions highlight the dynamic interplay between dissolved carbon dioxide, hydroxide ions, and aluminate species, ultimately leading to the formation of solid alumina hydrates.

$$CO_{2(g)} \rightarrow CO_{2(aq)} \quad (2)$$

$$CO_{2(aq)} + OH^-_{(aq)} \rightarrow HCO^-_{3(aq)} \quad (3)$$

$$HCO^-_{3(aq)} + OH^-_{(aq)} \rightarrow CO^{2-}_{3(aq)} + H_2O_{(l)} \quad (4)$$

$$Al(OH)^-_{4(aq)} \rightarrow AlOH_{3(s)} \downarrow + OH^-_{(aq)} \quad (5)$$

While carbonation offers a promising method for alumina hydrate recovery, several challenges must be addressed. High Na_2CO_3 concentrations in the solution, arising from incomplete leaching, excessive reagent use, or excessive CO_2 addition, can lead to the formation of dawsonite ($NaAlCO_3(OH)_2$), a sodium aluminate carbonate hydroxide. Dawsonite co-precipitates with alumina hydrates when Na_2CO_3 exceeds a critical concentration, reducing the purity of the final product and causing significant sodium losses [4]. Another concern is silicon co-precipitation. Silicate ions in the leach solution can lead to the incorporation of silicon into the precipitated product. Additionally, sodium ions may adsorb onto the surface of alumina hydrates, especially when sodium concentrations are high, further complicating downstream purification.

This study investigates the recovery of alumina from CA slags, a by-product of pyrometallurgical processes, via a carbonation-based route. The goal is to produce smelter-grade alumina (SGA) with a reduced environmental footprint. Key aspects examined include CO_2 consumption based on flow rate, the impact of seeding on particle size enhancement, the removal of residual soda and the calcination behavior of the alumina hydrates from alternative resources, contributing to a more sustainable and circular economy. Finally, the dissolution of the calcined alumina in cryolite is evaluated to assess its suitability for use in aluminium production.

2. Materials and Methods

2.1 Calcium Aluminate Slags

CA slags used in this study were produced from the pyrometallurgical reduction of various by-products and ores, including bauxite [5-7], bauxite residue [5, 8–10], calcium silicate slag [11–13], and manganese ore [14], within several EU-funded projects. A range of the main components of these slags is provided in Table 1. A high variation in composition is seen on most of the tested CA slags, reflecting the diverse feedstock materials.

Table 1. Calcium aluminate slag composition ranges from different raw materials [5-14].

Component (%)	Al_2O_3	CaO	SiO_2	Fe_2O_3	MgO	TiO_2	MnO	Na_2O	Cr_2O_3
Minimum	26.3	31.85	1.63	0.1	0.13	0.06	0.04	0.01	0.03
Maximum	52	53.9	17.53	5.41	4.05	7.31	6.47	2.7	0.11

2.2 Pregnant Leaching Solution

The CA slags were leached with Na_2CO_3 solution (ranging from 30-190 g/L of Na_2CO_3) under various conditions to produce PLS containing sodium aluminate, sodium carbonate, and sodium hydroxide. The range of the different PLS from different CA slags can be seen in Table 2.

Table 2. Range of pregnant leaching solutions produced [4, 5, 15, 16].

g/L	Na_2CO_3	NaOH	Al_2O_3	SiO_2
Minimum	0	3.1	15	0.2
Maximum	160	53.4	60	1

2.3 Carbonation Process

Carbonation of the PLS was conducted in a stirred tank reactor under controlled conditions, where CO_2 gas was continuously purged into the solution to induce the precipitation of alumina hydrates. The experimental setup has been described in detail in the authors' previous work [4, 17]. Specific operating conditions for each experiment are outlined in the respective sections. CO_2 off-gas measurements were recorded at one-second intervals, while the pH was monitored using a pH electrode (Endress & Hauser) equipped with a data logger, recording values at one-minute intervals. The resulting solid precipitates were dried at 110 °C for 24 hours and subsequently analyzed by X-ray diffraction (XRD). Liquid samples were analyzed using atomic absorption spectroscopy (AAS).

2.4 Water Washing

Multiple cycles of water washing were performed to remove the non-chemically bound Na ions from the produced alumina hydrate samples. Experiments were performed in a 50 mL glass reactor equipped with a vapor condenser to minimize volume loss. Once deionized water reached 90 °C, the hydrate was introduced and stirred at 300 rpm for 1 hour. The suspension was then filtered, and the filtrate was analyzed for sodium content via ICP-OES. The solid was dried, weighed, and subjected to further washing cycles. This process was repeated until sodium concentrations in the wash solution fell below detection limits.

2.5 Calcination

Calcination experiments were conducted on a sample precipitated from a pregnant leach solution derived from the sodium carbonate leaching of CA slag originating from the aluminothermic reduction of calcium silicate slag. No prior sodium removal treatment was applied. Thermal treatment was performed in a Nabatherm muffle furnace with electric resistance heating, using a heating rate of 5 °C/min to a predefined temperature and time.

2.6 Alumina Dissolution Testing Methodology

Alumina dissolution tests were carried out at SINTEF, on alumina samples produced in pilot plant operations at METLEN, Energy and Metals, under the EC funded projects ENSUREAL and SISAL PILOT. A standard SGA sample was used as a reference to assess differences in dissolution behavior.

In each test, 1 kg of industrial cryolite was melted in a graphite crucible at 980–983 °C and stirred at 80 RPM. After achieving stable readings for 5 minutes, 25 g of calcined alumina was added as a single batch through a steel tube. A submerged probe, operating on the critical current density (CCD) principle, was used to monitor the increase in dissolved alumina content. CCD values rise proportionally with alumina concentration. Bath samples were taken by briefly immersing a graphite rod into the melt surface and analyzed for oxygen content using a Leco ON-836 instrument. These results were used to calibrate the CCD measurements. It should be noted that bath samples may contain undissolved alumina, while the probe reflects only the dissolved fraction.

2.7 Analysis of Samples

Liquid samples: Aqueous solutions were analyzed for elemental composition by atomic absorption spectroscopy (AAS) with a PerkinElmer™ PinAAcle 900 T Atomic Adsorption Spectrometer and by inductively coupled plasma optical emission spectroscopy (ICP-OES) with PerkinElmer™ Optima 800.

Solid samples:
1) X-ray diffraction (XRD): patterns were acquired using a MiniFlex 600 benchtop diffractometer (Rigaku, Tokyo, Japan) equipped with a D/teX Ultra detector. The instrument operated at 40 kV and 15 mA (600 W), utilizing Cu-Kα radiation (Ni-filtered). Data were collected over a 2θ range of 10–75°, with a step size of 0.02° and a scanning rate of 5° (2θ) per minute. The mineralogical composition of the examined materials was determined using DIFFRAC. EVA V5.1 software (Bruker AXS, Karlsruhe, Germany) and the ICDD PDF-5+ 2024 and PDF-4 Minerals 2024 databases [18]. Quantitative phase analysis of the samples was performed using the fundamental parameters approach [19] in DIFFRAC.TOPAS V6 software (Bruker AXS, Karlsruhe, Germany). Initial structural models for the identified crystalline phases were obtained from the ICDD PDF-5+ 2024 and PDF-4 Minerals 2024 databases.
2) Electron microscopy and EDS: Morphological and elemental analysis was performed using a JEOL 6380LV SEM.
3) Chemical analysis: Alumina hydrate samples were chemically analyzed after aqua regia digestion.

3. Results

3.1 Carbonation

In previous work by the authors [4, 15], it was found that Na_2CO_3 concentration, CO_2 addition, and aging time significantly affect the precipitation behavior during the carbonation of sodium aluminate solutions. Below 40 g/L Na_2CO_3, alumina hydrates form; above 60 g/L, dawsonite dominates. When the Na_2CO_3 concentration is below 40 g/L, the formation of alumina hydrates is favored, while concentrations above 60 g/L lead predominantly to dawsonite precipitation. At an initial concentration of 20 g/L Na_2CO_3, extended carbonation duration enhances aluminium recovery, eventually resulting in nearly complete precipitation as dawsonite. Aging was found to further improve recovery by promoting the slow crystallization of alumina hydrates. The co-

precipitation of silicon with aluminium remains a critical challenge, necessitating careful control of the leaching and desilication processes.

To deepen the understanding of the carbonation process, this study investigates CO_2 gas consumption at varying flow rates and evaluates particle growth behavior and the effect of seeding.

3.1.1 CO_2 Consumption

To quantify CO_2 consumption during carbonation, experiments were conducted using a synthetic sodium aluminate solution under different gas flow rates: 40, 60, 80, 120, and 160 mLn/min. For comparison, a control experiment ("blank") was performed using a solution with the same NaOH and Na_2CO_3 concentrations, but without sodium aluminate ($NaAl(OH)_4$). The results are presented in Figure 1a–c.

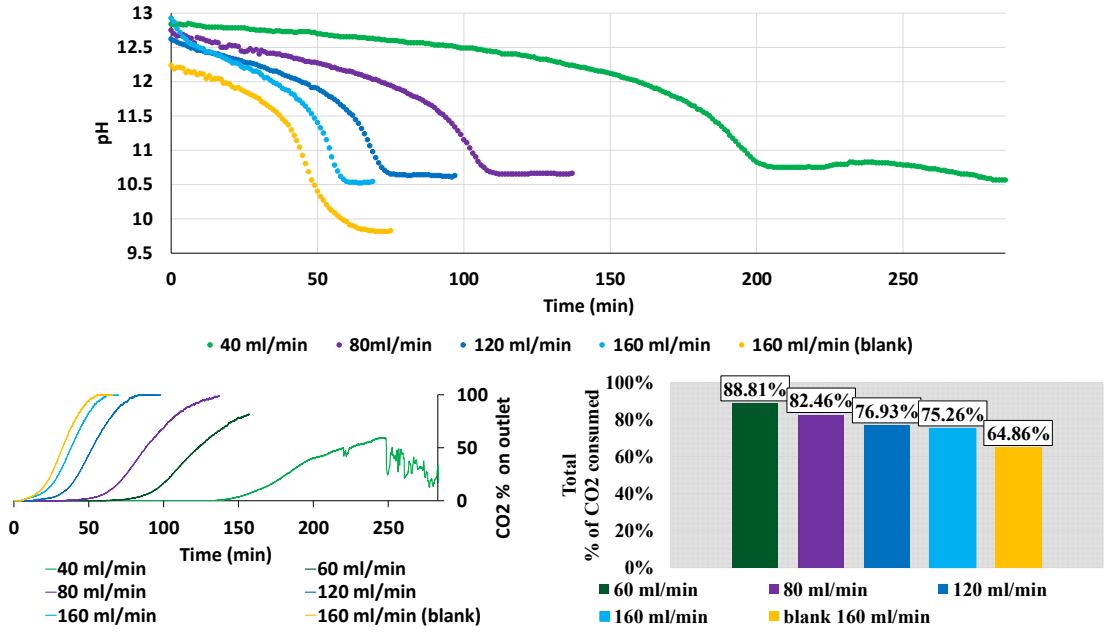

Figure 1. Carbonation in different flowrates. Top: pH measurements vs time, Bottom left: CO_2% measured on gas outflow composition vs time, Bottom right: Total CO_2 gas consumed.

[Conditions: Carbonation of synthetic SA solutions resulting from leaching CA slag from BR (starting solution: 20 g/L Na_2CO_3, 18.7 g/L NaOH, 15.1 g/L Al_2O_3, and 0.43 g/L SiO_2, gas: 99.995 % CO_2, Temperature: 40 °C and stirring: 200 rpm]

Figure 1 (top) shows the pH evolution for the different experiments. Initially, the pH decreases gradually due to the neutralization of free hydroxide ions. This is followed by a sharp drop, corresponding to the onset of alumina hydrate precipitation. As precipitation intensifies, the pH stabilizes, indicating a dynamic balance where the introduced H^+ ions are consumed by the hydroxide ions released during aluminium precipitation. Two key observations emerge: (i) higher CO_2 flow rates accelerate the onset of precipitation, and (ii) massive precipitation consistently begins within a pH range of 10.55–10.76. In the blank experiment (lacking aluminate ions), the pH profile parallels that of the 160 mL/min test until approximately pH 9.8. The absence of aluminate means no alkalinity is generated from precipitation, leading to a continued decline in pH. Figure 1 (bottom left) presents the CO_2 concentration in the outlet gas over time. As flow rate increases, a higher proportion of CO_2 exits unreacted, indicating insufficient contact time for gas-

liquid reaction. Figure 1 (bottom right) quantifies total CO_2 consumption per experiment. Comparison with the blank experiment reveals that the presence of aluminate ions results in approximately 10 % higher CO_2 uptake, attributed to the additional reaction pathways involved in alumina precipitation.

3.1.2 Seeding

For the seeding experiments, gibbsite of SGA-grade purity was used as the seed material. Nearly complete aluminium recovery (99.9 %) was achieved, with the newly precipitated phase comprising approximately 27 wt% of the total solid mass. XRD analysis identified gibbsite as the dominant phase in the precipitate, with minor traces of bayerite and nordstrandite. Notably, seeding not only enhanced precipitation efficiency but also steered phase selectivity toward gibbsite, replicating the seed's structure, whereas in unseeded systems, bayerite typically predominates [4, 15, 20]. According to the recent international patent application [21], this finding shows that the seeded precipitation generating gibbsite could only work in parallel with the Bayer process, as if no gibbsite is provided to be used as a seed material, the precipitate would be a mixture of alumina hydrates.

Table 3 presents the particle size distribution of the initial seed material and the final product. A slight increase in mean particle size from 89.86 to 91.9 µm was observed, suggesting both primary precipitation of new particles and secondary growth on existing crystals. The presence of smaller particles in the final product supports the occurrence of primary nucleation during carbonation.

SEM images in Figure 2 further illustrate these findings. In Figure 2 (left), newly formed needle-like alumina hydrate crystals can be seen nucleating on the surfaces of the hexagonal gibbsite seed particles. Figure 2 (centre) shows a crystal that grew from 80 to 120 µm after carbonation, indicating significant secondary precipitation and crystal growth. The morphology of the newly formed hydrates is predominantly needle-like, as shown in Figure 2 (right).

Table 3. Particle size distribution of seed and precipitate.

Sample	D (v, 0.1) (µm)	D (v, 0.5) (µm)	D (v, 0.9) (µm)
Gibbsite seed	55.63	89.86	127.59
Precipitate	12.04	91.90	131.96

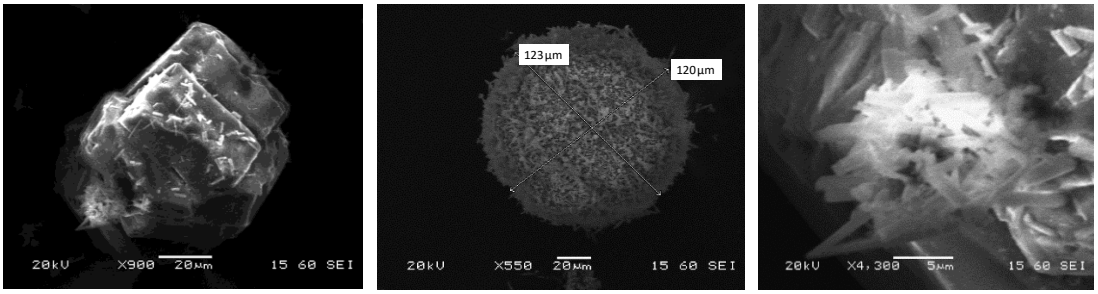

Figure 2. Scanning Electron Microscopy image of the alumina hydrate precipitate. Magnification: Left: x900, Center: x550, Right: x4300

[Conditions: Carbonation of sodium aluminate solution resulting from leaching CA slag from aluminothermic reduction of BR in pilot plant (starting solution: 24.5 g/L Na_2CO_3, 53.5 g/L, 46.3 g/L Al_2O_3 and 0.86 g/L SiO_2), mixture of gas CO_2/N_2 (20:80), gas flowrate: 176 mLn/min, Carbonation time: 7.73 h, Aging time: 13 h, Temperature: 60 °C and stirring: 200 RPM, seed addition: 20 % w/v. 99.9 % and 99 % Recovery of Al and Si, respectively]

3.2 Sodium Removal

The alumina hydrate sample used in these experiments was obtained from multiple carbonation tests performed on the pregnant leach solution (PLS) derived from the leaching of a calcium aluminate (CA) slag. This slag originated from the aluminothermic reduction of SiO_2 sand. XRD analysis confirmed the presence of bayerite, gibbsite, and nordstrandite in the precipitate. The chemical composition of the sample is shown in Table 4. Notably, the Na_2O content was measured at 1.66 %, which exceeds the typical maximum limit of 0.4 % for SGA [22, 23]. However, a recent study [24] suggests that a broader purity specification could tolerate Na_2O levels up to 0.6 %.

Table 4. Chemical composition of the alumina hydrate precipitate (on dry basis of calcined alumina).

Oxide	Al_2O_3	Fe_2O_3	SiO_2	CaO	Na_2O
%	96.7 ± 0.7	0.037 ± 0.015	0.24 ± 0.03	0.026 ± 0.0002	1.66 ± 0.05

The results of the water washing experiments are summarized in Figure 3. It was observed that lower pulp densities facilitated both a higher rate and a greater extent of sodium removal. Although the water-washable sodium fraction could be reduced to meet the broader purity limits suggested for alumina refineries [24], it remained above the strict requirement for SGA. In an industrial, continuous setup, significantly less water would be required per cycle. Furthermore, if a prior desilication step had been implemented, the amount of chemically bound sodium would likely be lower, as silicon tends to precipitate as sodium aluminosilicate compounds [25], from which sodium cannot be removed by simple washing but would require chemical treatment.

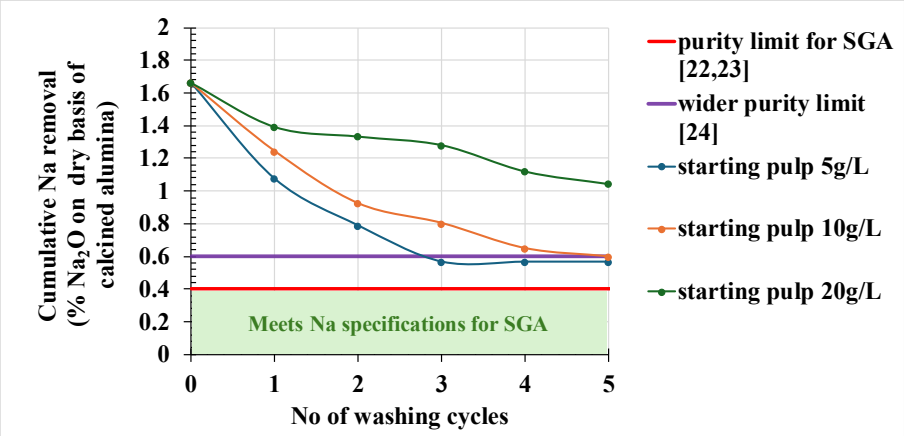

Figure 3. Sodium removal vs the No of cycles from the precipitated alumina hydrate mixture.

3.3 Calcination

The chemical composition of the alumina hydrate precipitate used in the calcination experiments is presented in Table 5, and its XRD pattern is shown in Figure 4. No seeding or sodium washing was applied prior to these experiments. The material primarily consists of bayerite, followed by gibbsite and a minor fraction of nordstrandite. SEM images of the uncalcined precipitate are displayed in Figure 5.

Table 5. Chemical composition of the alumina hydrate precipitate (on dry basis of calcined alumina).

Oxide	Al_2O_3	Fe_2O_3	SiO_2	CaO	Na_2O
%	98.8 ± 0.6	0.019 ± 0.005	0.42 ± 0.09	0.021 ± 0.002	0.75 ± 0.03

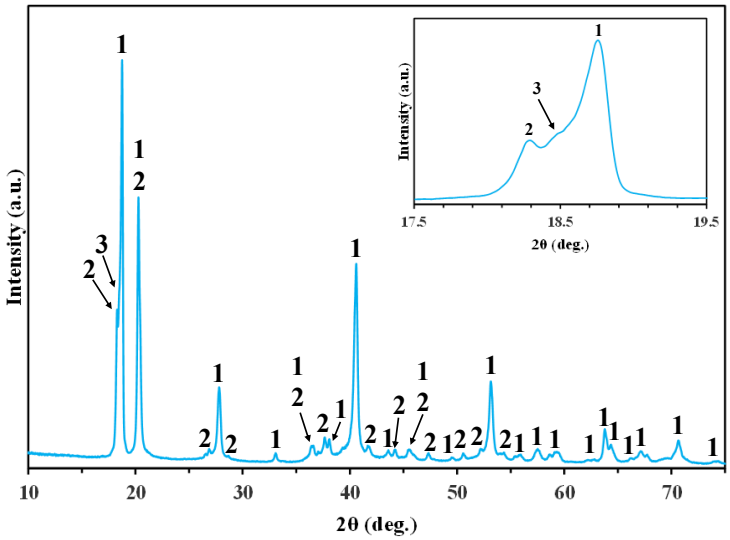

Figure 4. XRD pattern of the alumina hydrate precipitate (the onset in the figure shows the primary diffraction peak of the identified crystalline phases).

1. **Bayerite (75.6 %) [$Al(OH)_3$], 2. Gibbsite (20.8 %) [$Al(OH)_3$], 3. Nordstrandite (3.6 %) [$Al(OH)_3$]**

[Conditions: Carbonation of SA solutions resulting from leaching CA slag generated from aluminothermic reduction of calcium silicate slag (starting solution: 0 g/L Na_2CO_3, 28.6 g/L NaOH, 40.08 g/L Al_2O_3, and 0.24 g/L SiO_2), gas: 99.995 % CO_2, Temperature: 60 °C, and stirring: 200 RPM, 93 min of carbonation, 24 h aging]

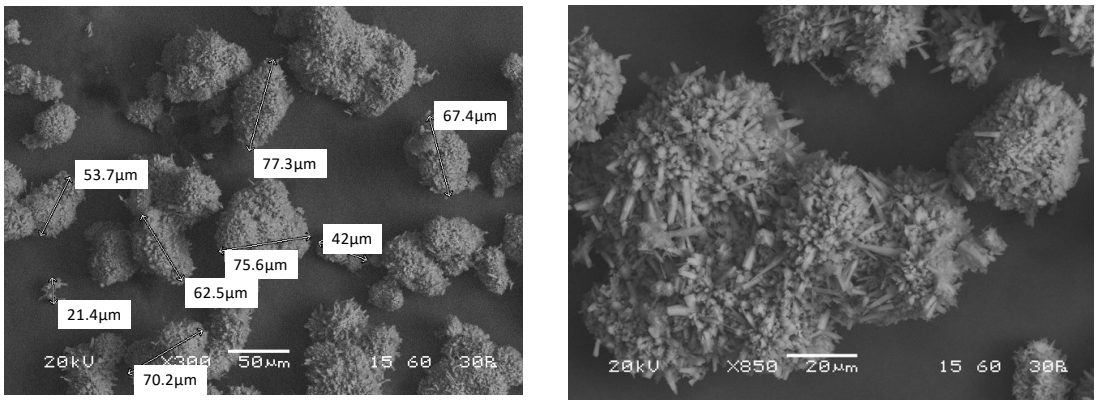

Figure 5. Scanning Electron Microscopy image of the alumina hydrate precipitate. Left: x300 magnification, Right: x850 magnification.

The alumina hydrate precipitate was calcined at various temperatures, and the resulting XRD patterns of the calcined products are presented in Figure 6 (left). At 300 °C, the transformation of trihydrate aluminas into monohydrate (boehmite) and non-stoichiometric transitional η-alumina is observed. By 400 °C, dehydration is complete, and the formation of transitional γ-alumina begins. At 1000 °C, θ- and κ-aluminas are detected, with their presence persisting at 1200 °C. These phase transitions align with established transformation pathways found in the literature: bayerite typically follows the sequence *boehmite* → $\eta \rightarrow \theta \rightarrow \alpha$, while gibbsite transitions through *boehmite* → $\chi \rightarrow \gamma \rightarrow \kappa \rightarrow \theta \rightarrow \alpha$ [26]. Nordstrandite is reported to follow a path similar to

bayerite [26]. Notably, χ-alumina was not detected in this study, diverging slightly from the expected gibbsite transformation route.

Additional calcination experiments were performed at 1200 °C with varying retention times (Figure 5, right). The results indicate that the α-alumina crystallizes at a short rate, even at 8 hours, transitional aluminas are still present. As proposed by Wijayarante et al. [27], this behaviour may be attributed to sodium impurities, as Na^+ ions are known to hinder the formation of α-alumina. This is consistent with the fact that the samples used in this study had not undergone extensive water washing prior to calcination.

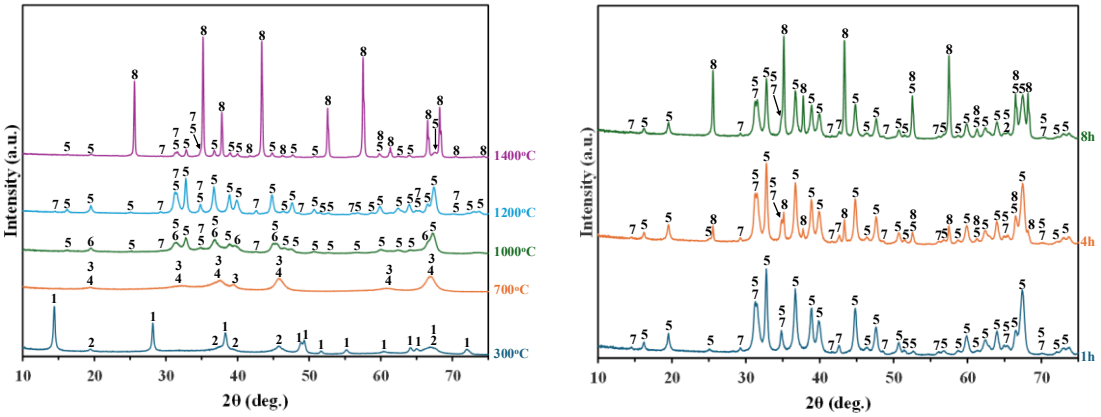

Figure 6. XRD patterns of calcined alumina hydrate precipitate. Left: at different temperatures, 1-hour retention time. Right: at 1200 °C for 1, 4, and 8 hours retention time.

1. **Boehmite [(AlO(OH)], 2. η-alumina [$Al_{2.667}O_4$], 3. η-alumina [$Al_{2.666}O_{3.999}$], 4. γ-alumina - $Al_{2.66}O_4$, 5. θ-alumina - Al_2O_3, 6. γ-alumina - Al_2O_3, 7. κ-alumina - Al_2O_3, 8. α-alumina - Al_2O_3**

3.4 Cryolite Dissolution

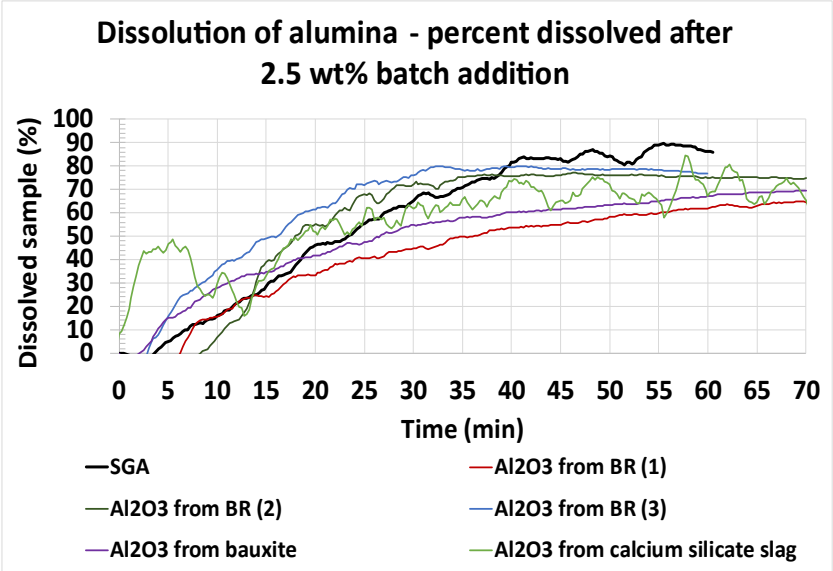

Figure 7. Comparison of the dissolution of calcined aluminas obtained from bauxite and BR smelting, and aluminothermic reduction of calcium silicate slag to the SGA sample.

The results of the dissolution test are presented in Figure 7. Calcined aluminas from different raw materials are presented. The tested samples showed lower reactivities compared to the SGA sample, however, this is still within acceptable limits. Concerning the alumina sample originating from calcium silicate slag, the initial probe response was a sharp rise and fall before steadily increasing. This initial response does not correspond to the amount of dissolved alumina, indicating that the probe was disturbed by the alumina addition.

4. Conclusions

This study highlights key process insights for alumina recovery from calcium aluminate slags via sodium carbonate leaching and carbonation. CO_2 consumption experiments showed that higher gas flowrate accelerates precipitation but reduces gas utilization efficiency, as unreacted CO_2 exits the system more rapidly. Seeding with gibbsite promoted both primary nucleation and secondary crystal growth. Prominently, seeding also directed the precipitating phase toward gibbsite, matching the seed material and enhancing phase selectivity.

Although the precipitated hydrates exhibited high Al_2O_2 content, their Na_2O levels exceeded SGA limits. Water washing effectively reduced Na_2O content to near industrial tolerance (0.6%), though not fully within standard SGA specifications. Calcination revealed typical phase transitions toward α-alumina at 1200 °C, with slower kinetics attributed to residual sodium impurities. Despite this, the final products demonstrated good dissolution behaviour in molten cryolite, comparable to standard SGA, confirming its potential as a viable alumina source pending further impurity control.

To sum up, if desilication is applied prior to carbonation and sodium removal becomes more effective, reducing the need for extensive water washing, there is a clear potential for scalable and sustainable alumina production from calcium aluminate slags, with promising applicability in the aluminium industry. The remaining consideration is whether differences in precipitate morphology could pose operational challenges, which warrants further investigation.

5. Acknowledgements

This work has been completed in the course of the European Union's Horizon 2020 research and innovation programs: ENSUREAL (GA No 767533), SiSal Pilot under (GA No 869268) and HAlMan (GA No 101091936).

6. References

1. Javier Bullon et al., Separation Time of Aluminothermic Reduction Products for Sustainable Silicon Production, *Open Research Europe*, 4, (2024), 249, htpps://doi.org/10.12688/openreseurope.18833.2
2. Michail Vafeias et al., From red to grey: revisiting the Pedersen process to achieve holistic bauxite ore utilisation, *2nd International Bauxite Residue Valorisation and Best Practices Conference* 2018: Athens, Greece, 109-115.
3. Morris L. Roberson, John W. Beck, Jack S. Maples et al., *Bayer process production of alumina*, K.A.a.C. Corp., US Patent 4,036,931, 1977.
4. Danai Marinos et al., Carbonation of Sodium Aluminate/Sodium Carbonate Solutions for Precipitation of Alumina Hydrates—Avoiding Dawsonite Formation, *Crystals*, 11, 7, (2021), 836,
5. James Malumbo Mwase et al., Investigating Aluminium Tri-Hydroxide Production from Sodium Aluminate Solutions in the Pedersen Process, *Processes*, 10, 7, (2022), 1370,
6. Fabian Imanasa Azof and Jafar Safarian, Leaching kinetics and mechanism of slag produced from smelting-reduction of bauxite for alumina recovery, *Hydrometallurgy*, 195, (2020). htpps://doi.org/10.1016/j.hydromet.2020.105388

7. Adamantia Lazou et al., High Temperature Treatment of Selected Iron Rich Bauxite Ores to Produce Calcium Aluminate Slags, *Materials Proceedings*, 5(1), (2021), 36. https://doi.org/10.3390/materproc2021005036
8. Michail Vafeias et al., Alkaline alumina recovery from bauxite residue slags, *3rd International Bauxite Residue Valorization and Best Practices Conference*, Virtual, 2020, 55-62
9. Michail Vafeias et al., Leaching of Ca-Rich Slags Produced from Reductive Smelting of Bauxite Residue with Na2CO3 Solutions for Alumina Extraction: Lab and Pilot Scale Experiments, *Minerals*, 11, 8, (2021), 10.3390/min11080896.
10. Pritii Tam et al.,Carbothermic Reduction of Bauxite Residue for Iron Recovery and Subsequent Aluminium Recovery from Slag Leaching, *35th Interantional ICSOBA Conference*, Hamburg, Germany, 2017, p. 603-613
11. Aikaterini Toli et al., Sustainable Silicon and High Purity Alumina Production from Secondary Silicon and Aluminium Raw Materials through the Innovative SisAl Technology, *Materials Proceedings*, 5, 1, (2021), 85,
12. Georgia Maria Tsaousi et al., Control of Silica Gel Formation in the Acidic Leaching of Calcium Aluminate Slags with Aqueous HCl for Al Extraction, *Sustainability*, 15, 21, (2023), https://doi.org/10.3390/su152115462.
13. Zhu Mengyi and Jafar Safarian, Alumina Production from CaO-Al2O3-SiO2 Slag Produced in SisAl Process, *41st International ICSOBA Conference*, United Arab Emirates, Dubai, 5-9 November, 2023, p. 499-509
14. *HAlMan project, https://halman-project.eu/*. 101091936.
15. Danai Marinos et al., Parameters Affecting the Precipitation of Al Phases from Aluminate Solutions of the Pedersen Process: The Effect of Carbonate Content, *Journal of Sustainable Metallurgy*, 7, 3, (2021), 874-882, 10.1007/s40831-021-00403-w.
16. Eirini Georgala et al., Aluminium extraction from a calcium aluminate slag using sodium carbonate based on the critical examination of the patented industrial Pedersen process, *Hydrometallurgy*, 222, (2023), https://doi.org/10.1016/j.hydromet.2023.106188.
17. Giorgos Gakis, et al., An Integrated, CFD-Based, Analysis of Carbonation in a Stirred Tank Reactor, *Materials*, 18, (2025), 1535, 10.3390/ma18071535.
18. Stacy Gates-Rector and Thomas Blanton, The Powder Diffraction File: a quality materials characterization database, *Powder Diffraction*, 34, 4, (2019), 352-360, 10.1017/S0885715619000812.
19. R. W. Cheary and A. Coelho, A fundamental parameters approach to X-ray line-profile fitting, *Journal of Applied Crystallography*, 25, 2, (1992), 109-121, 10.1107/s0021889891010804.
20. Valeh Aghazadeh, Somayeh Shayanfar and Abdoullah Samiee Beyragh, Thermodynamic Modeling and Experimental Studies of Bayerite Precipitation from Aluminate Solution: Temperature and pH Effect, *Iranian Journal of Chemistry and Chemical Engineering (IJCCE)*, 38, 2, (2019), 229-238, 10.30492/ijcce.2019.30926.
21. David Konlechner et al., Method for the production of aluminium hydroxide from bauxite, *International Patent Application published under the Patent Cooperation Treaty (PCT)*, M.S.A, Editor. 2022: WO2023/133601 A1
22. Stephen J. Lindsay, Customer Impacts of Na2O and CaO in Smelter Grade Alumina, *Light Metals 2012*, C.E. Suarez, Editor. 2016, Springer International Publishing: Cham. p. 163-167.
23. Benny E. Raahauge, Smelter Grade Alumina Quality in 40+ Year Perspective: Where to from Here?, in *Light Metals 2015*, M. Hyland, Editor. 2016, Springer International Publishing: Cham. p. 73-78.
24. Stephen Lindsay, Alumina Properties and Challenges Ahead *41st International ICSOBA Conference*, Dubai, 2023, 153-163.
25. James Malumbo Mwase and Jafar Safarian, Desilication of Sodium Aluminate Solutions from the Alkaline Leaching of Calcium-Aluminate Slags, *Processes*, 10, 9, (2022), 1769,

26. Margaret K. B. Day and Vernon J. Hill, Thermal Transformations of the Aluminas and their Hydrates, *Nature*, 170, 4326, (1952), 539-539, 10.1038/170539a0.
27. Hasini Wijayaratne et al., Balancing Sodium Impurities in Alumina for Improved Properties, *Metallurgical and Materials Transactions B*, 49, 5, (2018), 2809-2820, 10.1007/s11663-018-1310-z.